iScience

CellPress
OPEN ACCESS

Article

The increasing atmospheric CO_2 over India: Comparison to global trends

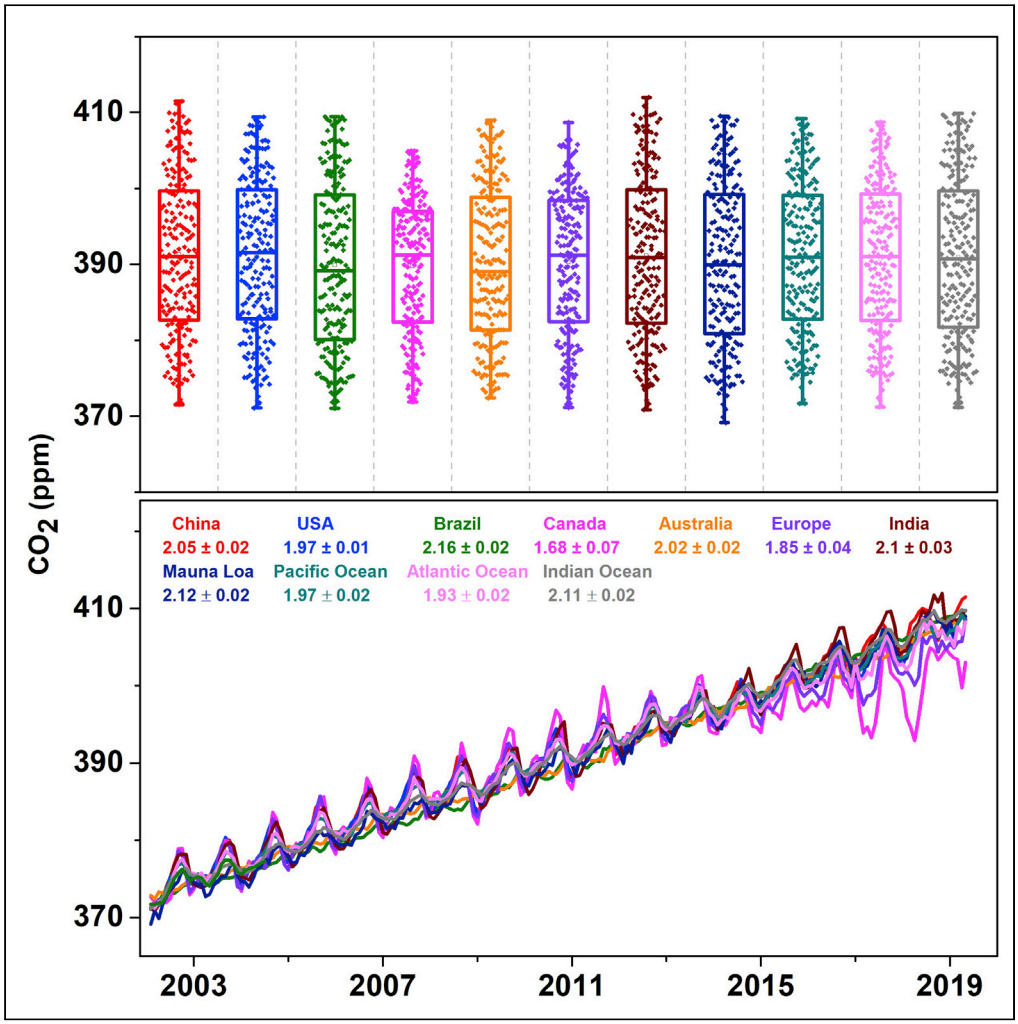

Jayanarayanan Kuttippurath, Rony Peter, Ajay Singh, Sarath Raj

jayan@coral.iitkgp.ac.in

Highlights

All satellite CO_2 measurements show a bias between −0.5 and 3.0 ppm

Coastal India shows high concentrations and the highest trend is 2.4 ppm/yr

The global average CO_2 trends are similar to that of India, about 1.8-2.1 ppm/yr

The Increasing CO_2 is a concern for regional warming and global climate change

Kuttippurath et al., iScience 25, 104863
August 19, 2022
https://doi.org/10.1016/j.isci.2022.104863

iScience

CellPress
OPEN ACCESS

Article

The increasing atmospheric CO_2 over India: Comparison to global trends

Jayanarayanan Kuttippurath,[1,2,*] Rony Peter,[1] Ajay Singh,[1] and Sarath Raj[1]

SUMMARY

Atmospheric CO_2 is the key Greenhouse Gas in terms of its global warming potential and anthropogenic sources. Therefore, it is important to analyze the changes in the concentration of atmospheric CO_2 to monitor regional and global climate change. Here, we use ground-based and satellite measurements for the 2002-2020 period to assess CO_2 over India. The average CO_2 trend over India is about 2.1 ppm/yr, and the highest trends are in agreement with the increase in total energy consumption during the period, and the highest trends are found in the areas of mines and refineries in the west and east India. The estimated CO_2 trends for India are comparable to that of global tropical and mid-latitude regions. The increasing CO_2 implies serious anthropogenic global warming and thus, calls for mitigation measures and continuous monitoring for timely policy interventions.

INTRODUCTION

Carbon dioxide (CO_2) has a very prominent role in the regulation of Earth's temperature (Hegerl et al., 2006; Foster et al., 2017). Apart from being one of the key greenhouse gases (GHGs), it also plays an important part in the plant and animal processes (i.e., photosynthesis and respiration) and thus, is responsible for the changes in climate (Apadula et al., 2019; Ekwurzel et al., 2017; Wang, 1999; IPCC, 2007). The atmospheric concentration of CO_2 depends on the exchange of carbon fluxes among its sources and sinks. The major sources include fossil fuel burning, biological respiration, and change in land-use patterns, whereas the terrestrial biosphere and oceans are the most important sinks that regulate the amount of CO_2 in the atmosphere (Houghton 1998; Gunter et al., 1998). There has been a substantial rise in atmospheric CO_2 in the past 150 years, from 280 to 416 ppm (Krishnapriya et al., 2020), owing to the industrial activities that support modern human civilization. These increasing levels of CO_2 lead to changes in global radiative forcing and climate (IPCC, 2007; 2021). Therefore, reducing CO_2 emissions should be one of the main goals to mitigate anthropogenic climate change (Thompson et al., 2016).

As the focus of current scientific research is mostly anthropogenic climate change and GHGs, it is very important to understand the changes in CO_2 concentrations caused by human activities and natural environment for future climate predictions (Cui et al., 2020; Sanghavi et al., 2020; Raj et al., 2020). To monitor the CO_2 concentrations, high-precision station-based surface observations are used. On average, the oceans and terrestrial biosphere absorb about 60% of the anthropogenic CO_2 emissions, and 40% remain in the atmosphere (IPCC, 2014). The environment modifies these atmospheric concentrations, but monitoring those changes with *in situ* measurements is very expensive and time-consuming (Bousquet et al., 1996). Additionally, these estimates are inadequate to represent and assess the regional and global carbon fluxes; leaving critical scientific questions related to the carbon cycle unanswered (Boesch et al., 2011; IPCC, 2021). The practice of making use of space-based observations is the best way to achieve this, as measurements from space-borne instruments have global coverage in high frequency. The temporal evolution of trace gases in the atmosphere can also be tracked simultaneously in different parts of the earth by satellites.

There are different space-based approaches for estimating the atmospheric concentrations of CO_2. The differential absorption technique is the first approach, which makes use of absorption wavelengths of CO_2 in SWIR (Short Wave Infrared) (Bréon and Ciais, 2010). Some satellite instruments use the thermal infrared (TIR) channels for CO_2 observations. Additionally, solar occultation methods are applied in some other instruments (Patra et al., 2008; Sioris et al., 2014; Foucher et al., 2011). The SWIR-based

[1]CORAL, Indian Institute of Technology Kharagpur, Kharagpur 721302, India

[2]Lead contact

*Correspondence: jayan@coral.iitkgp.ac.in

https://doi.org/10.1016/j.isci.2022.104863

Table 1. The specifications of satellite measurements used in this study

Dataset	Satellite	Spatial coverage	Processing level	Spatial resolution	Temporal range
Atmospheric InfraRed Sounder (AIRS)	Earth Observing System (EOS) Aqua	90°N –60°S; 180°W - 180°E	3	2° × 2.5°	2002-09-01 to 2017-03-01
Thermal And Near infrared Sensor for carbon Observation - Fourier Trans-form Spectrometer (TANSO-FTS)	Greenhouse Gases Observing Satellite (GOSAT)	90°N –90°S; 180°W - 180°E	3	2.5° × 2.5°	2009-06-01 to 2020-01-31
Scanning Imaging Absorption spectrometer (SCIAMACHY)	ENVISAT	90°N –90°S; 180°W - 180°E	2	L2 regridded to 2.5° × 2.5°	2002-08-02 to 2012-04-08
Orbiting Carbon Observatory-2 (OCO-2)	NASA OCO-2	90°N –90° S; 180°W, 180°E	2	L2 regridded to 2.5° × 2.5°	2014-09-06 to 2020-01-31

observations have more sensitivity at the surface, but the TIR measurements have sensitivity throughout the troposphere (Chédin et al., 2003; Peter et al., 2021).

The scanning imaging absorption spectrometer for atmospheric cartography (SCIAMACHY) was the first satellite to measure atmospheric CO_2, which was launched on the Environmental Satellite in March 2002. Afterward, NASA (National Aeronautics Space Administration) launched AIRS (Atmospheric Infrared Sounder) onboard Aqua in May 2002 (e.g. Chédin et al., 2003). The Thermal And Near infrared Sensor for carbon Observation - Fourier Trans-form Spectrometer (TANSO-FTS) on Greenhouse gases Observing SATellite (GOSAT) was the project put forward to measure CH_4 and CO_2 from space using infrared channels (Yoshida et al., 2012) and was launched in 2009. Recently, NASA launched its first exclusive CO_2 mission in July 2014, the Orbiting Carbon Observatory (OCO) – 2 (Miller et al., 2007; Crisp et al., 2004). In addition, TES (Tropospheric Emission Spectrometer) onboard the Aura satellite is also employed to observe atmospheric CO_2 from 2004 onward (Kulawik et al., 2010, 2013). Infrared Atmospheric Sounding Interferometer (IASI) onboard MetOp-A (Meteorological Operational satellite program), launched into orbit in 2006, has spectral attributes similar to that of TES, but the measurements are performed mostly in the tropics (20° S-20° N) (Crevoisier et al., 2009). Further details about the measurements are given in Table 1.

In recent decades, the fossil-fuel CO_2 emissions from India have shown an annual increase of +7% (Boden et al., 2009). According to Thompson et al. (2016), fossil fuel emissions increased between 1990 and 2010 by 190% in India (to 0.55 PgC per year; 1 PgC = 1×10^{15} g carbon in CO_2). It is mainly contributed by the cement production, transport, electricity, and power generation sectors. Past studies used ground-based (Tiwari et al., 2011, 2013) and aircraft-borne (Baker et al., 2011; Nayak et al., 2011) measurements, and model simulations (e.g. Valsala et al., 2013; Patra et al., 2011, 2013) to analyze atmospheric CO_2 in India. In addition, flask measurements are also performed to estimate the GHG concentrations in the Himalaya and western India regions (Anthwal et al., 2009; Sharma et al., 2014; Mahesh et al., 2016). Recently, Gupta et al. (2019) presented the spatial and temporal changes in mid-tropospheric CO_2 over India for the period 2002-2011. They reported a noticeable seasonal and inter-annual variability in CO_2 over India, and estimated a trend of 2.01 ppm/yr in their study period.

As the measurements and analyses of atmospheric CO_2 over India are limited, in-depth studies are inevitable for detecting anthropogenic warming and climate change driven by GHGs (e.g. Preethi et al., 2011; Patel and Kuttippurath, 2022). Henceforth, we present the spatial and temporal changes in atmospheric CO_2 over India using multi-satellite measurements for the past 19 years (2002-2020). In addition, we have also estimated the trends in global atmospheric CO_2 using ground-based and satellite observations. The trends in CO_2 are assessed with the auxiliary data of temperature, precipitation, vegetation, and emission data from industries, mining, energy, and power sectors. It is the first comprehensive study of its kind, as the analyses also include multi-satellite bias estimates to make robust statistics of long-term trends in CO_2 for policy decisions. This is particularly significant in the context of the Paris Climate Agreement.

RESULTS AND DISCUSSION

Figure 1 demonstrates the satellite measurements and their ability to capture the seasonal and temporal changes in atmospheric CO_2. SCIAMACHY is the first space-borne instrument to observe atmospheric CO_2

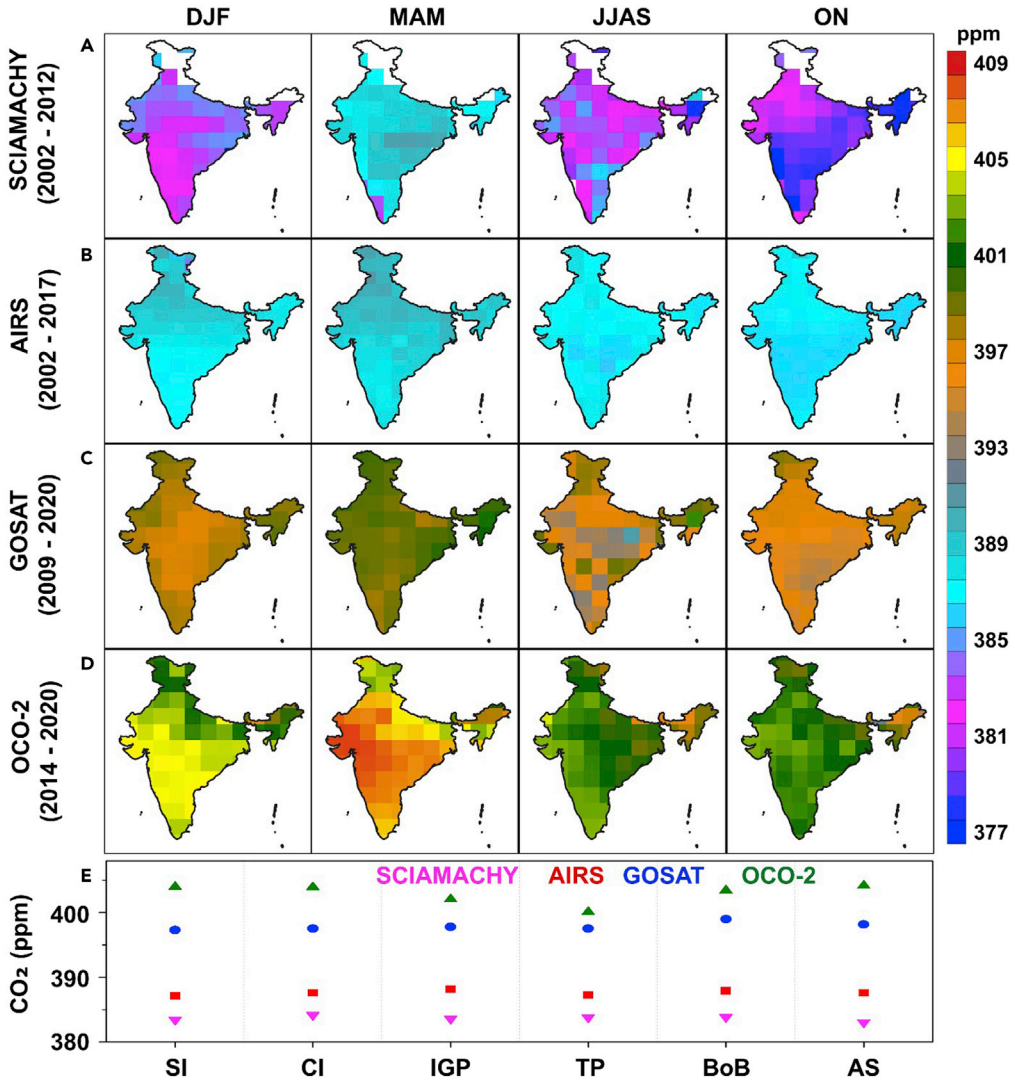

Figure 1. Space-borne observations of CO_2

The seasonal distribution of atmospheric CO_2 concentrations in India as measured by the satellite instruments (A) SCIAMACHY, (B) AIRS, (C) GOSAT, and (D) OCO-2. The seasons are defined as winter (DJF), summer (MAM), monsoon (JJAS, summer or southwest monsoon), and autumn (ON, post-monsoon or northeast monsoon). (E) The regions in the bottom panel are: SI is South India, CI is Central India, IGP is Indo-Gangetic Plain, TP is the Third Pole, BoB is the Bay of Bengal and AS is the Arabian Sea.

and was launched in 2002 and decommissioned in 2012. Therefore, the average CO_2 concentrations are lower than that of any other satellite measurements here. The OCO-2 and GOSAT are the recently launched satellite payloads and are currently operating. Therefore, their measurements show higher CO_2 concentrations than that of SCIAMACHY and AIRS in all seasons. Figure 1E compares the annual averaged CO_2 concentrations from each satellite, in which the gradual progression in atmospheric CO_2 in each satellite observation period is very clear in all regions. The SCIAMACHY measurements show the lowest (385 ppm) and OCO-2 shows the highest (410 ppm) CO_2 values among the measurements, as explained previously. All satellite measurements show distinct and similar seasonal variability, illustrating the consistency in observations by different instruments. The highest values are found in MAM (March-May, summer) and the lowest in JJAS (June-September, monsoon) seasons. The seasonal difference is within 4 ppm and is consistent with all satellite measurements. Indian land area is very vast, and the topography and vegetation cover are different and diverse. Henceforth, it is expected that the seasonal distribution of CO_2 to be slightly different in different parts of India. This makes the October-November (ON, northeast monsoon

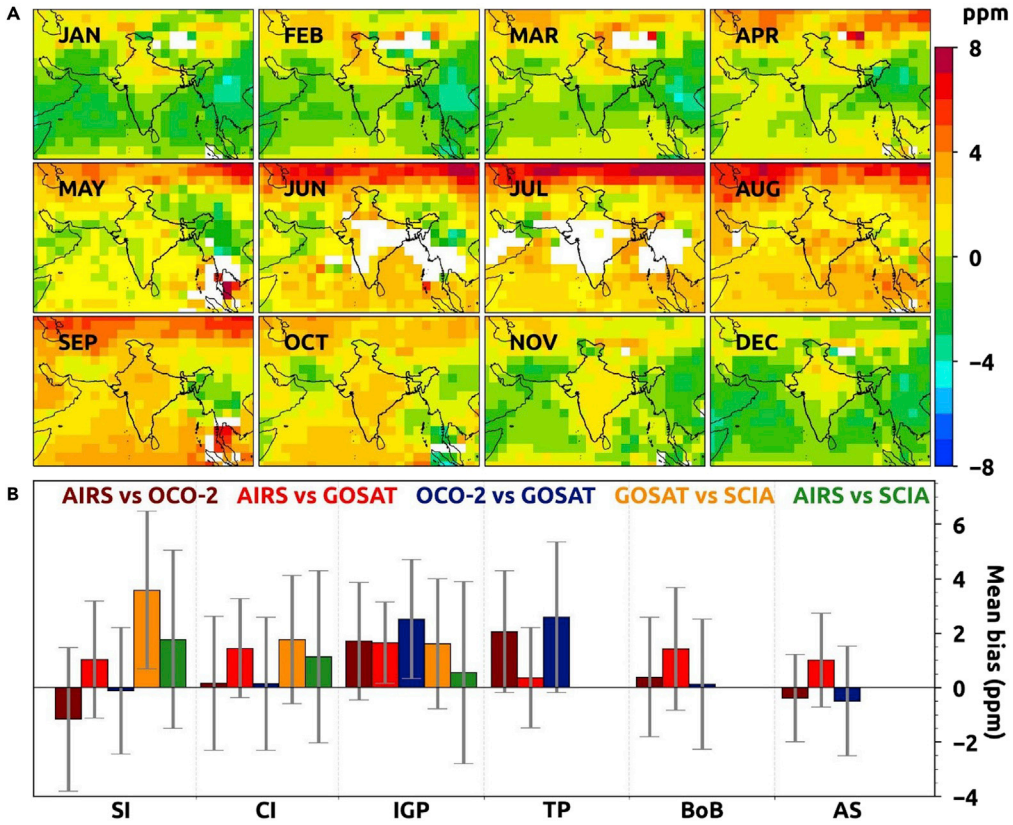

Figure 2. Bias in different satellite CO_2 measurements

(A) The monthly averaged bias calculated between AIRS and GOSAT CO_2 concentrations over India and adjacent continental and oceanic regions.

(B) The bias calculated for different homogeneous regions in India and nearby continental and oceanic regions, where SI is southern India, CI is central India, IGP is Indo-Gangetic Plains, TP is Third Pole, BB is the Bay of Bengal, and AS is the Arabian Sea. The vertical bars represent the SD from the mean. The regions are marked in Figures S5 and S6.

season) measurements show the lowest CO_2 values in some regions. Similarly, the CO_2 concentrations are relatively higher in the north and east than that in south India. The regional differences are about 8 ppm and are congruent in all satellite measurements. Therefore, these concatenated data for the period 2002-2020 can be used for scientific studies and are suitable for long-term trend calculations. However, the inter-annual analyses consider the complete year, and therefore, the measurements from 2003 to 2019 are considered. We have estimated the bias between the satellite measurements and use the combined data for further scientific discussion.

Bias estimates

Atmospheric Infrared Sounder and Greenhouse gases Observing SATellite (ARGO)

The monthly bias calculated between the overlapping years of AIRS and GOSAT is depicted in Figure 2. The differences are smaller compared to the distinct seasonal differences in the bias. The smallest bias is observed in DJF (December, January, and March) with less than +2 ppm over the land, whereas the Indian Ocean and Southeast Asia regions exhibit −2 to 0 ppm. The differences are highest in MAM, particularly north of 30° N latitude. The very small negative bias observed over southeast Asia in NH (Northern Hemisphere) decreases with time. A relatively higher bias (>5 ppm) is observed north of 30° N and the whole region has a positive bias greater than 3 ppm in JJAS. The bias again reduces to 1-2 ppm over the land and even smaller over the ocean during ON. The large difference in monsoon months is primarily owing to the increase in CO_2 intake by vegetation, which reduces the CO_2 levels near the surface. This immediate reduction is not found in the mid-troposphere; making higher bias there. The presence of the subtropical jet stream has also a role in transporting the atmospheric CO_2 to the higher latitudes.

Atmospheric Infrared Sounder and Orbiting Carbon Observatory-2 (AROC)

Figure S1 shows the bias estimated between AIRS and OCO-2. During DJF, the Indian Ocean exhibits negative bias, whereas the land regions show positive values, and the bias is within 3 ppm. A higher positive bias is observed during the monsoon months of JJAS, mainly to the north of 30° N and the average bias is in the range of 3-5 ppm. This higher bias is similar to that found between AIRS and GOSAT. The bias decreases and reverses over the ocean, and is within −2 to −1 ppm in ON. This is owing to the transport of surface emissions toward the oceanic regions by the northeast monsoon winds, which do not usually affect the mid and upper tropospheric CO_2 distribution.

Atmospheric Infrared Sounder and SCanningImaging Absorption spectroMeter for Atmospheric CartograpHY (ARSC)

The smallest differences are found in the winter months, about 1 ppm as shown in Figure S2. As SCIAMACHY measurements are sensitive at the surface, it captures the seasonality of atmospheric CO_2 more prominently as compared to AIRS. One to two months lag in the seasonal variability of CO_2 is observed for AIRS, which is also not as strong as that in SCIAMACHY or other satellite observations. The CO_2 concentration measured by SCIAMACHY is smaller than that of the mid-troposphere by AIRS in MAM. In JJAS, the reduction in atmospheric CO_2 because of the vegetation intake makes higher bias over the land and at higher latitudes. The difference decreases from October to November with an average bias within ± 2 ppm.

Greenhouse Gases Observing Satellite and Orbiting Carbon Observatory-2 (GOOC)

GOSAT and OCO-2 are currently operating satellites that measure atmospheric CO_2. The bias calculations are shown in Figure S3. In general, the comparisons show a large bias over the land regions, and the bias increases to 6 ppm, except for MAM and JJAS. The bias is relatively small in the rainy seasons (JJAS and ON), within ± 2 ppm. Note that the measurements are sporadic in JJAS, which makes fewer data available to compare over the land regions.

Greenhouse Gases Observing Satellite and SCanningImagingAbsorption spectroMeter forAtmospheric CartograpHY (GOSC)

SCIAMACHY CO_2 measurements are higher than that of GOSAT in almost all months. The comparison shows a difference within ± 2 ppm over all land regions, as depicted in Figure S4. However, the difference is about −8 ppm over the eastern India in some months. As the data are not available over the oceanic and plateau regions, bias calculations are not performed for those areas.

We have discussed the differences in atmospheric CO_2 measured by different satellites across the latitudes. Therefore, we have also found the mean CO_2 concentrations in homogeneous regions, and are illustrated in Figure S5. The largest mean bias is observed for GOSC, about 3.5 ppm. Over the land regions, Central India shows the lowest bias, with a peak of 2 ppm for GOSC and the smallest difference of 0.5 ppm for GOOC. Both oceanic basins exhibit a similar magnitude in mean bias, but the difference is negative for AS in the comparisons of AROC and GOOC. Ocean basins show a smaller bias than that over the land, with the highest mean bias of 1.4 ppm in BoB for ARGO and the lowest of 0.15 ppm in BoB for GOOC. This regional analysis suggests that the largest bias is about 3.5 ppm and the smallest at about 0.15 ppm. Compared to the accuracy of the individual satellite measurements, about 1-2 ppm, depending on the instruments, the bias (from −1.0 to 3.5 ppm) is not large and the measurements are well suited for scientific analyses.

Atmospheric CO_2 over India: Spatial and temporal changes

Atmospheric CO_2 has a direct connection to anthropogenic activities. Although it is a well-mixed GHG, the changes in fossil fuel burning and vegetation affect its variability in the atmosphere, as shown in Figure 3. The emission from land-use changes is one of the largest human-made sources of CO_2 (Le Quéré et al., 2009). Furthermore, the highly industrialized regions show high CO_2 values, such as eastern India (Figure S6 shows different regions in India). Similarly, relatively lower values are observed in the places where deforestation is severe. Logging and deforestation emit CO_2, but are partly offset by CO_2 uptake by the secondary vegetation. Northeast India (NEI) with higher values of about 407 ppm is an example for such areas, but about 3 ppm more in other regions. Note that deforestation is the second largest source of anthropogenic CO_2 after fossil fuel combustion (e.g. van der Werf et al., 2009).

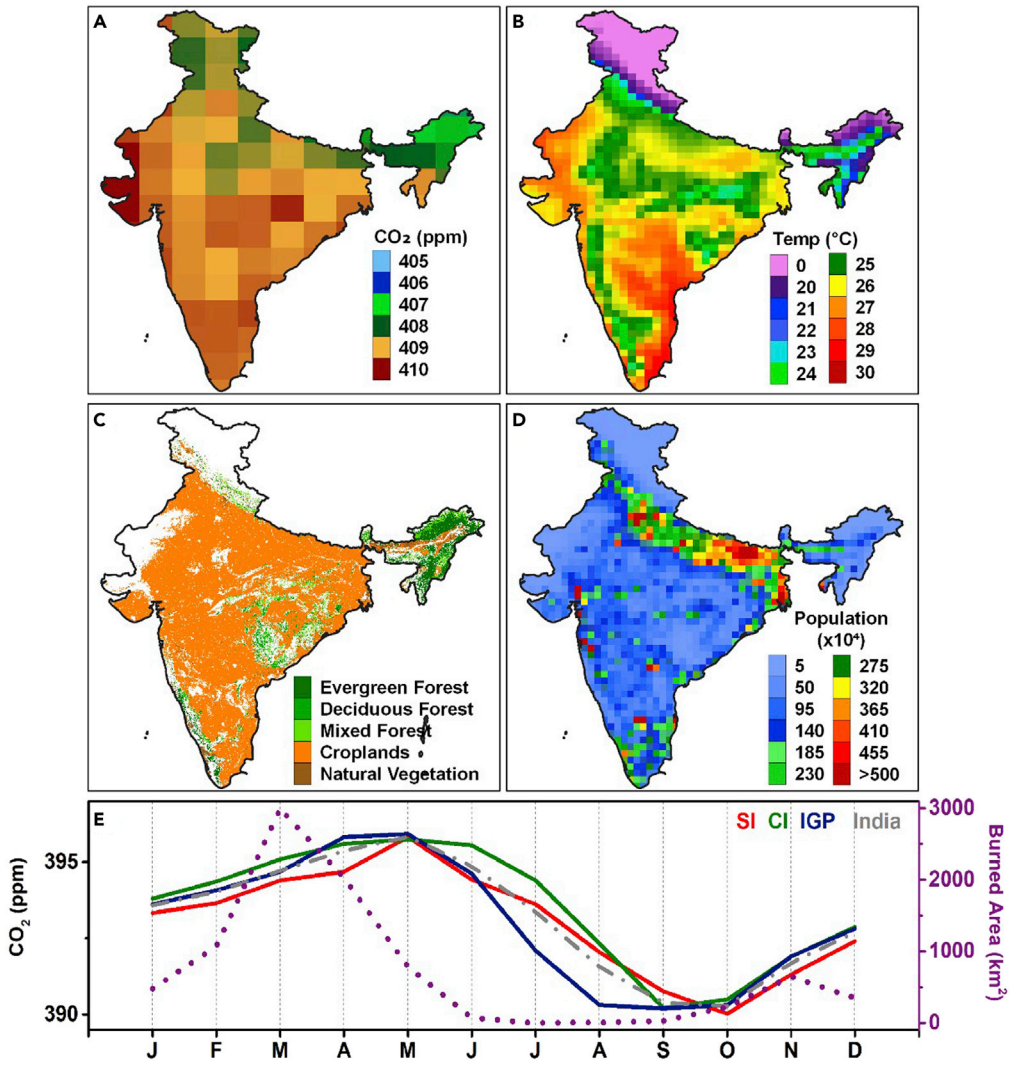

Figure 3. The spatial distribution of CO_2 and selected drivers

The annual-averaged CO_2 concentrations in India as estimated from available satellite measurements during the period 2002-2020. The satellite measurements include SCIAMACHY, AIRS, GOSAT, and OCO-2. The annual-averaged temperature, land use, and population are also depicted. The monthly distribution of annual CO_2 in different regions of India are shown in the bottom panel. The regions SI are southern India, CI is Central India, IGP is Indo-Gangetic Plain is IGP and all India averaged data (India). The first letter of each month is shown on the X axis of the bottom panel (e.g. starting from J – January to D – December).

There is a distinct seasonal variability in CO_2 distribution over India and is illustrated in Figure 4. The smallest concentrations are found in JJAS and then in ON, i.e during the monsoon rainfall months. The highest concentrations are found in MAM and DJF. The difference between JJAS and MAM is about 8-9 ppm, and that between DJF and MAM is about 4 ppm. However, the difference in CO_2 concentration between the monsoon months is about 1-2 ppm. In all cases, the largest concentration among the regions is found in the northeast and southeast India.

The summer months with higher temperatures and dry weather make the ecosystems to reduce the exchange of carbon and thus, the MAM months show the highest CO_2 concentrations (Patra et al., 2013). In addition, most croplands are left fallow in this season owing to the unavailability of farm irrigation and this reduces vegetation and suppresses the carbon sink pathways. The comparatively slow winds in this season inhibit transport and mixing, which also makes higher CO_2 there (Sharma et al., 2013). On the other hand, the monsoon months with high precipitation and enhanced soil moisture produce more photosynthetic activity and thus higher sink of CO_2.

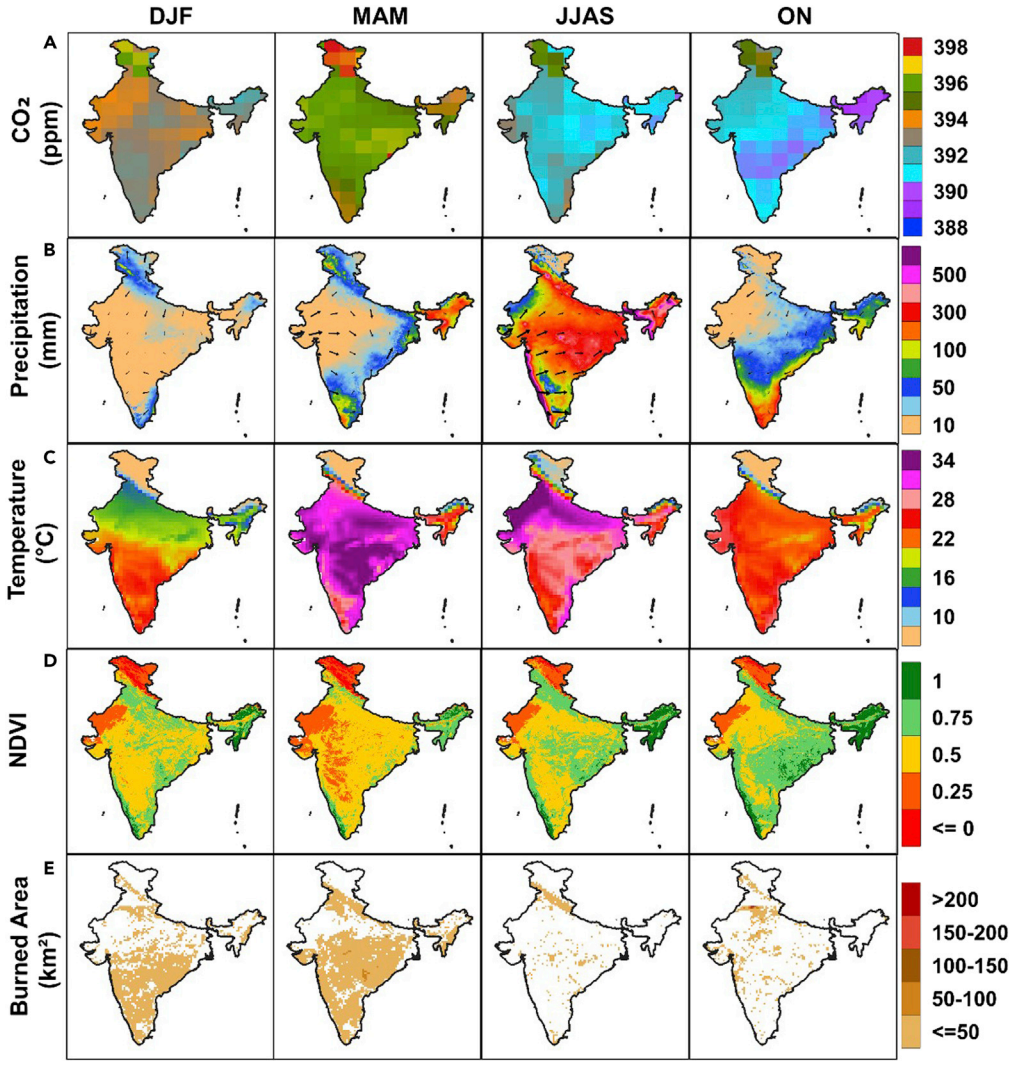

Figure 4. Seasonal variability of atmospheric CO_2 over India and key drivers

(A) The seasonal changes in atmospheric CO_2 concentrations over India as estimated from available satellite measurements during the period 2002-2020. The satellite measurements include SCIAMACHY, AIRS, GOSAT, and OCO-2. The corresponding seasonal distribution of (B) precipitation (winds overlaid), (C) temperature, (D) NDVI, and (E) burned area is also illustrated.

Additionally, as southwest monsoon (JJAS) brings about 75% of total rainfall in India (Oza and Kishtawal, 2014), agriculture greatly depends on this rainfall. The intense agriculture activities make more crops and vegetation, and these would produce more sink for CO_2. This is also reflected in the NDVI (Normalized Difference Vegetation Index) data. Distinct seasonal variability and a strong relationship between NDVI and CO_2 are observed in all four seasons, as demonstrated in Figure 4. There is a high anti-correlation between NDVI and CO_2 (e.g. Gupta et al., 2019). The presence of dense monsoon clouds blocks sun radiation and reduces the temperature, decreases the soil and leaf respiration, and increases carbon uptake. After JJAS, the lowest CO_2 concentrations are found in ON, which is also the northeast monsoon season. The east coast of India receives half of its annual rainfall in this season, and the Rabi crops are grown during this period. In addition, the peninsular region has most of its rainfall during JJAS, and thus, these areas show smaller CO_2 concentrations in this season (Gupta et al., 2019).

The concentration of CO_2 gradually increases by DJF as the winter months approach. Winters demand more power and heating systems. The heating consumes large amounts of fossil fuels, and thus a significant amount of CO_2 is emitted to the atmosphere. As the plants are dormant during winter, weak photosynthesis and strong respiration contribute to relatively high levels of CO_2. The regional

distribution of atmospheric CO_2 over India shows a consistent pattern in all seasons. NEI and Hilly areas show the highest, and the Peninsular region exhibits the smallest CO_2 concentrations in all seasons. All four satellites show a similar distribution of atmospheric CO_2. However, as the satellites were launched in different years, the absolute values of CO_2 are different. For instance, the first satellite that measured atmospheric CO_2 was SCIAMACHY. Therefore, CO_2 values show then maximum, about 384 ppm, and the difference is about 8-9 ppm with the average values shown by other satellite measurements.

Biomass burning is an important source of atmospheric CO_2 (Yang and Zhao, 2019; Shi et al., 2017; Singh et al., 2022). We have used the burned area (Figure 3E) as a proxy for biomass burning. There are many fire events in India, particularly at NEI, Indo-Gangetic Plain (IGP), hilly regions of east and Kashmir, and Central India. We have taken the total burned area in all Indian regions for each month here. The burned areas show large seasonal variability, from 0 to 3000 km^2. The largest burned areas are found in the dry months of February, March, and April, about 2000 km^2. There is a second peak in October and November, but the amount of burned area is ten times smaller, about 250-500 km^2. Both peaks are influenced by the annual cycle in fires corresponding to the Kharif and Rabi harvest seasons, respectively (e.g. Kuttippurath et al., 2020). The agriculture-intensive regions such as IGP have two peaks, as depicted in the figure. Conversely, the eastern and northeastern regions have the peak fire events in October and November. In addition, the peaks in February-March in the peninsular region are in agreement with the harvest season there (e.g. Singh et al., 2021; Venkataraman et al., 2006). Therefore, the highest values in atmospheric CO_2 coincide with the peaks in biomass burning in India. The time lag in CO_2 peaks with that of the burned areas can be owing to the spatial averaging of the data. This is further illustrated in Figure 4E, where the spatial distribution of burned areas is presented. The analyses show very small burned areas or fire events in spring and monsoon seasons, but large areas, except the northernmost states such as Kashmir, are under fire events in winter and autumn as discussed with Figure 3E. The shifting cultivation is still practiced in the northeast India, for which the primary and secondary forests are cleared through a slash and burn process and then the crops are cultivated after 1-3 years. Therefore, higher CO_2 concentration is observed in those regions (Pasha et al., 2020). Furthermore, it is reported that the burning of 63 Mt of crop stubble releases about 3.4 Mt of CO, 0.1 Mt of NO_x, 91 Mt of CO_2, 0.6 Mt of CH_4, and 1.2 Mt of particulate matter to the atmosphere (Abdurrahman et al., 2020). Therefore, biomass burning also contributes to the higher emissions of CO_2 in India.

Trends in CO_2 over India

The inter-annual variability of atmospheric CO_2 exhibits a constant and consistent rise from the year 2003 onward, as shown in Figure 5. The year 2003 has a value of about 370 ppm, which increased to 410 ppm by 2019. This suggests that there has been an increase of 40 ppm in 17 years. In addition to the spatial changes, we have also estimated the average CO_2 in different regions such as the IGP, south, and north India. For instance, the illustration demonstrates the Keeling curve for IGP, where measurements from different satellites are shown. All satellite measurements agree with the increasing trends in atmospheric CO_2 across the seasons. All satellite data and the seasonal averages show similar trend values of about 2 ppm/yr. In these years, the fossil fuel consumption of India has rapidly increased owing to the economic development in the country (Kuttippurath et al., 2022). The consumption of crude oil increased by 50% during the last decade in India (Ministry of Petroleum and Natural Gas, India, https://mopng.gov.in/en). Furthermore, India ranks second for coal consumption globally, and there was a continuous increase in its consumption between 2008 and 2017 (Office of Coal Controller, Ministry of Coal, India, http://www.coalcontroller.gov.in/). Apart from these, cement production and total energy consumption have contributed substantially to this increase in CO_2. The trend in atmospheric CO_2 is also directly influenced by land-use changes. After the industrialization in 1850, enhanced anthropogenic activities and changes in land-use patterns led to the degradation of soil and thus, made huge emissions of CO_2 to the atmosphere (Smith et al., 2007). Furthermore, India's agricultural land use CO_2 emissions also show an increasing trend from 2009 to 2017 (Singh et al., 2022).

We have estimated the linear trends in CO_2 over the period, as shown in Figure 6. It shows a gradual increase in atmospheric CO_2 in all regions. Therefore, we quantified the trends in atmospheric CO_2 over India for the past 17 years. The highest trends are found in DJF, about 2.1-2.4 ppm/yr. The trends in ON are similar, but 0.1-0.2 ppm/yr smaller than that in DJF. The smallest trends among the seasons are found in JJAS, about 1.8-2.0 ppm/yr. On the other hand, the trends in MAM vary between 1.8 and 2.4 ppm/yr, depending on the region. The lowest regional trends are found in the east and northeast India, about 1.8-1.9 ppm/yr. Our results are consistent with that of Gupta et al. (2019), who reported an increasing trend of 2.01 ppm/yr in AIRS CO_2 over India

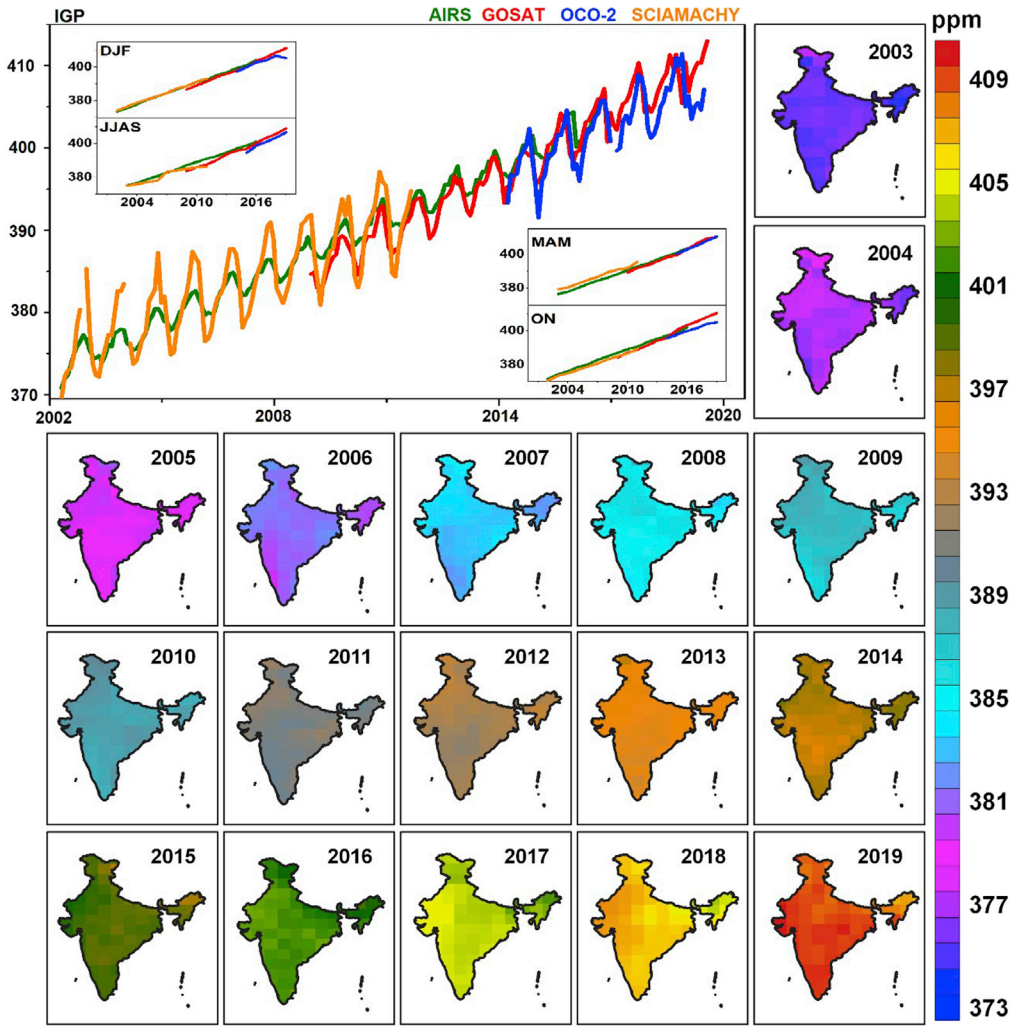

Figure 5. The Keeling Curve and Inter-annual variability of atmospheric CO_2 in India

The yearly distribution of atmospheric CO_2 concentrations in India as estimated from available satellite measurements during the period 2002-2019. The averaged data (maps) include SCIAMACHY, AIRS, GOSAT, and OCO-2 measurements. The Keeling curve (top left) for the Indo-Gangetic Plain (IGP) region for the annual and seasonal data.

between 2003 and 2011. The regional trends are in agreement with the anthropogenic sources of atmospheric CO_2 there. For example, the largest trends found on the western coast, north of eastern coast, and south of northeast are in accordance with a large number of mines and refineries there (Figure 6). The positive trends are also in accordance with the increasing trends in oil, gas, coal, and total energy consumption, as illustrated in the figure. Nevertheless, the vegetation shows a small negative trend and therefore, the sink of CO_2 is reduced during the period, but is masked by the anthropogenic sources. The relatively lower anthropogenic source regions, such as South India, show smaller CO_2 trends.

Comparison with global CO_2 trends across the latitudes

We have compared the CO_2 trends in India to that of other regions in the world (Figure 7). The mean CO_2 shows about 390-391 ppm in the tropics and mid-latitudes in the northern hemisphere. The rate of increase in CO_2 concentration is significantly higher in NH than that in SH, and higher over land than over the oceans. The southern tropical and mid-latitude regions show about 388-389 ppm, and the Polar regions exhibit about 387-388 ppm. The trends estimated across the latitudes show about 2.0-2.1 ppm/yr from 10° S to 50° N and the highest trends are observed over the Arabian Sea, Eastern Asia, and Northern Africa. The smallest trends are computed for the Arctic, about 1.5 ppm/yr. Our results agree with that of Cao et al. (2019), who also presented a similar spatiotemporal distribution of global CO_2. Apart from these, we have averaged the satellite CO_2 over specific locations with

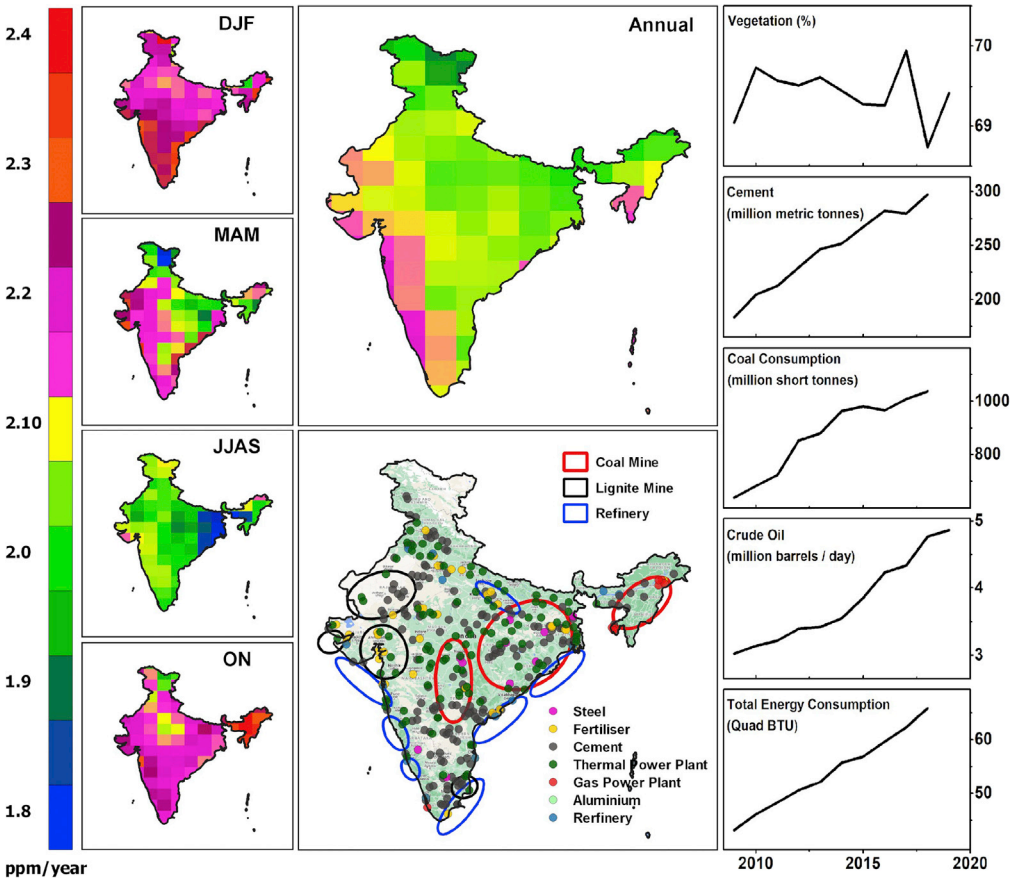

Figure 6. Seasonal and annual trends in atmospheric CO_2

Trends in atmospheric CO_2 concentrations over India as estimated from available satellite measurements during the period 2002-2020. All trends are statistically significant at the 95% confidence interval. The averaged data include SCIAMACHY, AIRS, GOSAT, and OCO-2 satellite measurements. The yearly distribution of Vegetation, Cement Production, Coal, Crude Oil, and Total Energy Consumption from 2008 to 2019 in India are also shown. The elongated circles in the maps represent the industry regions such as coal mines and refineries.

long-term surface data, as illustrated in the figure (bottom panel). For instance, the Mauna Loa surface measurements compare well with the Hawaii satellite measurements and the CO_2 concentration is about 416 ppm in 2021 there. The long-term trends show similar values, about 2.14 ppm/yr in the past two decades, but 1.82 ppm/yr in 1979-2020. The satellite measurements at Mount Waliguan, Gobabeb, and Wendover agree very well with the surface CO_2 measurements, about 412-415 ppm in 2021 in these regions. The estimated trends show about 2.06, 2.28, and 2.12 ppm/yr, respectively, and both satellite and surface measurements show similar trend values for the common observation period. In short, the trends in global CO_2 are also in agreement with that estimated over India and are around 2.1 ppm/yr.

We have also assessed the global CO_2 concentrations by averaging the satellite data from different countries, regions, and oceans. The results are shown in Figure 8, where the top panel shows the mean values over the observation period (2002-2020) and their SD (standard deviation). The trend and its significance at the 95% confidence interval in different regions are shown in the second panel from the top. The third panel shows the temporal evolution of atmospheric CO_2 over different regions. The bottom panel shows the change in power sector emissions in the world since 2010. The figure illustrates that the mean values are around 390 ppm and there are only slight differences among the selected regions. The time series shows a similar temporal evolution of atmospheric CO_2 in all regions. However, Brazil, Australia, and the Indian Ocean hardly exhibit seasonal variability, as found for the Kenya station. This suggests that the CO_2 is well mixed and no new seasonal sources exist in these regions. Conversely, high seasonal variability is observed in all other regions. Interestingly, there has been a slowdown in CO_2 concentration since 2011

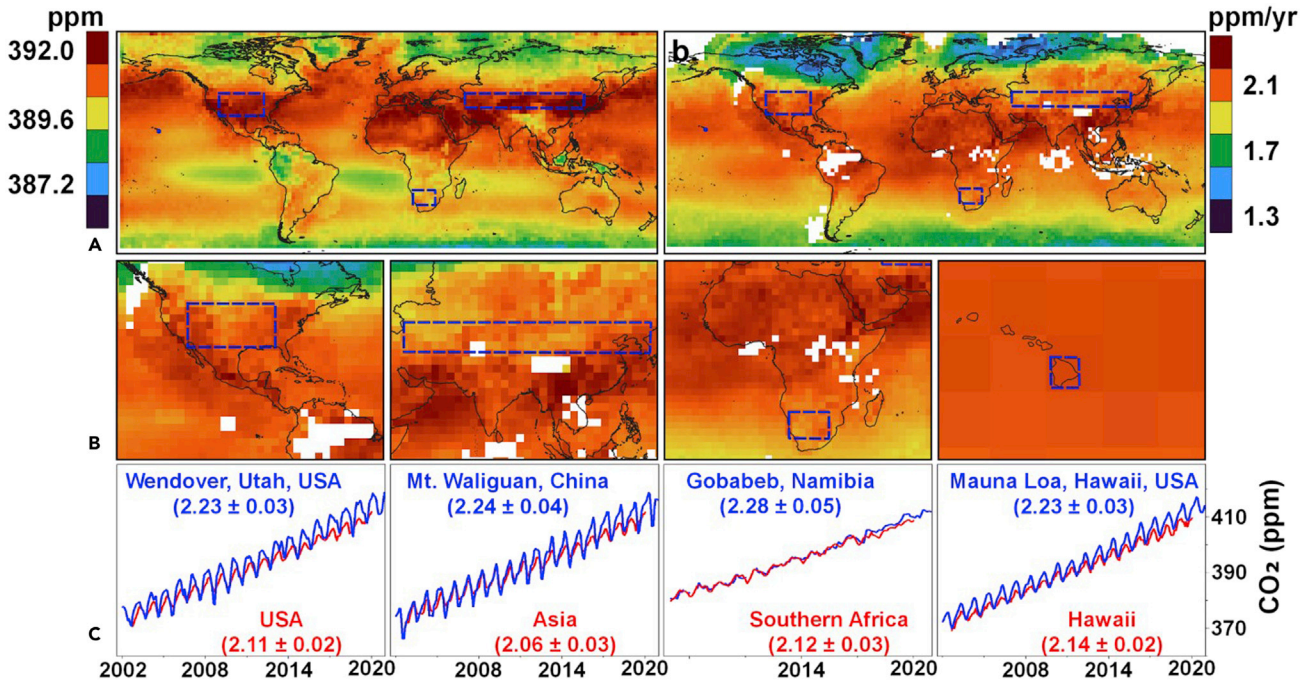

Figure 7. Global CO_2 Observations

(A) The average (top left) and trend (top right) in atmospheric CO_2 concentrations across the globe as estimated from the averaged satellite measurements during the period 2002-2020. The averaged data include SCIAMACHY, AIRS, GOSAT, and OCO-2 satellite measurements. (B) The analysis of satellite measurements in different regions is also shown. The selected regions are marked in blue boxes and those averaged data are compared to the nearby surface station measurements in the bottom panels (B and C).

in all regions, which is stronger in Canada, Europe, the USA, and the Atlantic Ocean from 2015 onwards. Our findings are consistent with that of Olivier and Peters (2019), who reported a slower growth rate in global CO_2 emissions in 2015 and 2016 (0 and +0.3%, respectively). This decrease is mainly owing to the decline in global coal consumption driven by the three years (2014-2016) of decreasing coal consumption in China, the USA, and Europe, owing to the increased renewable power generation there. In addition, Jackson et al. (2017) also reported that CO_2 emissions were stable for the period 2015-2017, despite the continuing growth in the global economy. The smallest declining trends are observed in Canada and the highest in Brazil (about 2.16 ppm/yr). India, China, Mauna Loa, and Australia show similar trends of about 2.0-2.12 ppm/yr. Among the oceanic regions, the Indian Ocean shows the highest increase of about 2.11 ppm/yr, which is equal to that of the continental regions. The global average trend is about 1.85 ppm/yr and is higher than that of Canada and Europe, but nearly equal to that of the Atlantic and Pacific Oceans. In brief, the atmospheric CO_2 shows a decrease from 2011 onward as compared to its immediate previous decades. Note that all trends mentioned above are statistically significant at the 95% confidence interval.

As discussed previously, there was a slowdown in the increase of atmospheric CO_2 across the latitudes from 2010 to 2015, which is consistent with the decline in the global power sector emissions (bottom panel). All four main energy sectors show a consistent decrease in associated emissions throughout the period (e.g. Kuttippurath et al., 2022). These declining trends in power sector emissions have been continuing and the change was very high during the 2016-2020 period. The largest reduction in power sector emissions is observed for the year 2020 and is owing to the lockdown restrictions with the COVID-19 pandemic. This suggests that the pandemic has further helped the global environment to reduce the burden of atmospheric CO_2 (Le Quéré et al., 2020; Sikarwar et al., 2021).

Conclusions

We examine the distribution of atmospheric CO_2 over India using four different space-borne measurements and their averaged data over the past 19 years (2002-2020). The measurements show a bias of about −0.5 to 3 ppm, and most satellites show positive bias, and the lowest bias is estimated over the oceanic

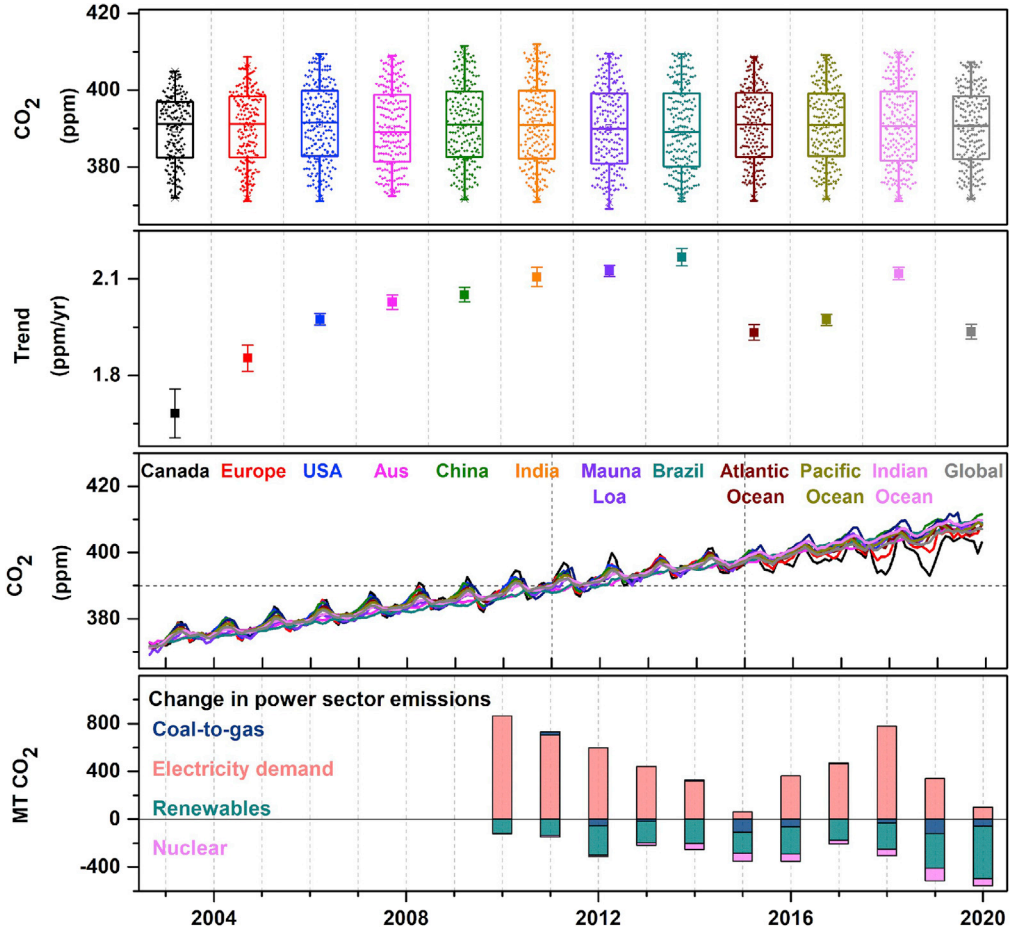

Figure 8. Trends in global CO_2

The mean (top) and trend (second panel from the top) in atmospheric CO_2 concentrations in different regions of the world (marked in the third panel from the top) are estimated from the averaged satellite measurements during the period 2002-2020. The averaged data include SCIAMACHY, AIRS, GOSAT, and OCO-2 satellite measurements. The boxplots show the mean and deviations from the mean for the observation period. The changes in power sector emissions are shown in the bottom panel.

regions and southern India. The highest concentrations are observed in summer and the lowest in monsoon months, and the seasonal variability is largely in accordance with the precipitation and vegetation changes during the period. All seasons and measurements show similar temporal evolution and trends, and the average trend is about 2.1 ppm/yr. The seasonal trends are largest in winter and autumn, at about 2.3 ppm/yr. The highest trends coincide with the energy consumption, mining, and refinery regions in western and eastern India. Li et al. (2022) described that coal is one of the main industries causing carbon emissions. Therefore, regulating these emissions can play a vital role in reducing or controlling the atmospheric CO_2 in India. In addition, a decreasing trend in the vegetation is also observed during the period. The analyses of global CO_2 show similar trend values as that for India and are within 1.8-2.2 ppm/yr. The ever-increasing atmospheric CO_2 is a serious concern for climate change and global warming, and therefore, warrants constant monitoring, mitigation measures, and policy decisions.

Limitations of the study

We have not estimated the emissions using the Inversion modeling. This will be presented in a separate work as this analysis is intended to address the CO_2 concentrations in different regions in India and across the globe from multiple satellite and ground-based observations. This is the first step to examine the global CO_2 emissions to analyze its spatiotemporal differences in its radiative forcing and global warming potential.

STAR★METHODS

Detailed methods are provided in the online version of this paper and include the following:

- KEY RESOURCES TABLE
- RESOURCE AVAILABILITY
  - Lead contact
  - Materials availability
  - Data and code availability
- METHOD DETAILS
  - Datasets
  - Methods
- QUANTIFICATION AND STATISTICAL ANALYSIS

SUPPLEMENTAL INFORMATION

Supplemental information can be found online at https://doi.org/10.1016/j.isci.2022.104863.

ACKNOWLEDGMENTS

We thank the Chairman CORAL, the Director of Indian Institute of Technology Kharagpur (IIT KGP), the Ministry of Education (MoE), National Center for Ocean Information Services (INCOIS), Hyderabad, and the Ministry of Earth Science (MoES, O-MASCOT project) for facilitating the study. We also thank all the data managers and the scientists who made available those data for this study. This study did not receive any funding from any agencies or institutions.

AUTHOR CONTRIBUTIONS

JK: Conceptualization, Methodology, Software, Validation, Formal analysis, Investigation, Resources, Data Curation, Writing - Original Draft, Writing - Review & Editing, Visualization, Supervision, Project administration, Funding acquisition: RP, AS, SR: Methodology, Software, Validation, Formal analysis, Investigation, Data Curation, Visualization, Writing – Original Draft.

DECLARATION OF INTERESTS

The authors declare no competing interests.

Received: February 12, 2022
Revised: May 28, 2022
Accepted: July 27, 2022
Published: August 19, 2022

REFERENCES

Abdurrahman, M.I., Chaki, S., and Saini, G. (2020). Stubble burning: effects on health & environment, regulations and management practices. Environ. Adv. *2*, 100011. https://doi.org/10.1016/j.envadv.2020.100011.

Anthwal, A., Joshi, V., Joshi, S., Sharma, A., and Kim, K.-H. (2009). Atmospheric carbon dioxide levels in Garhwal Himalaya, India. J. Korean Earth Sci. Soc. *30*, 588–597. https://doi.org/10.5467/jkess.2009.30.5.588.

Apadula, F., Cassardo, C., Ferrarese, S., Heltai, D., and Lanza, A. (2019). Thirty years of atmospheric CO_2 observations at the Plateau Rosa station, Italy. Atmosphere *10*, 418. https://doi.org/10.3390/atmos10070418.

Aumann, H.H., Chahine, M.T., Gautier, C., Goldberg, M.D., Kalnay, E., McMillin, L.M., Revercomb, H., Rosenkranz, P.W., Smith, W.L., Staelin, D.H., et al. (2003). AIRS/AMSU/HSB on the aqua mission: design, science objectives, data products, and processing systems. IEEE Trans. Geosci. Remote Sens. *41*, 253–264. https://doi.org/10.1109/TGRS.2002.808356.

Baker, A.K., Schuck, T.J., Slemr, F., Van Velthoven, P., Zahn, A., and Brenninkmeijer, C.A.M. (2011). Characterization of non-methane hydrocarbons in Asian summer monsoon outflow observed by the CARIBIC aircraft. Atmos. Chem. Phys. *11*, 503–518. https://doi.org/10.5194/acp-11-503-2011.

Boden, T.A., Marland, G., and Andres, R.J. (2009). Global, Regional, and National Fossil-Fuel CO_2 Emissions (Carbon dioxide information analysis center, Oak ridge National Labaratory). https://doi.org/10.3334/CDIAC/00001_V2010.

Boesch, H., Baker, D., Connor, B., Crisp, D., and Miller, C. (2011). Global characterization of CO_2 column retrievals from shortwave-infrared satellite observations of the Orbiting Carbon Observatory-2 mission. Remote Sens. (Basel). *3*, 270–304. https://doi.org/10.3390/rs3020270.

Bovensmann, H., Burrows, J.P., Buchwitz, M., Frerick, J., Noël, S., Rozanov, V.V., Chance, K.V., and Goede, A.P.H. (1999). SCIAMACHY: mission objectives and measurement modes. J. Atmos. Sci. *56*, 127–150. https://doi.org/10.1175/1520-0469(1999)056<0127:SMOAMM>2.0.CO;2.

Bousquet, P., Ciais, P., Monfray, P., Balkansk1, Y., Ramonet, M., and Tans, P. (1996). Influence of two atmospheric transport models in inferring sources and sinks of atmospheric CO_2. Tellus B *48*, 568–582. https://doi.org/10.1034/j.1600-0889.1996.t01-2-00011.x.

Bréon, F.M., and Ciais, P. (2010). Spaceborne remote sensing of greenhouse gas concentrations. Compt. Rendus Geosci. *342*, 412–424. https://doi.org/10.1016/j.crte.2009.09.012.

Cao, L., Chen, X., Zhang, C., Kurban, A., Qian, J., Pan, T., Yin, Z., Qin, X., Ochege, F.U., and Maeyer, P.D. (2019). The global spatiotemporal distribution of the mid-tropospheric CO_2 concentration and analysis of the controlling factors. Remote Sens. (Basel). *11*, 94. https://doi.org/10.3390/rs11010094.

Chahine, M., Barnet, C., Olsen, E.T., Chen, L., and Maddy, E. (2005). On the determination of atmospheric minor gases by the method of vanishing partial derivatives with application to CO_2. Geophys. Res. Lett. *32*, L22803. https://doi.org/10.1029/2005GL024165.

Chahine, M.T., Chen, L., Dimotakis, P., Jiang, X., Li, Q., Olsen, E.T., Pagano, T., Randerson, J., and Yung, Y.L. (2008). Satellite remote sounding of mid-tropospheric CO_2. Geophys. Res. Lett. *35*, L17807. https://doi.org/10.1029/2008GL035022.

Chédin, A., Saunders, R., Hollingsworth, A., Scott, N., Matricardi, M., Etcheto, J., Clerbaux, C., Armante, R., and Crevoisier, C. (2003). The feasibility of monitoring CO_2 from high-resolution infrared sounders. J. Geophys. Res. *108*, 1–19. https://doi.org/10.1029/2001jd001443.

Crevoisier, C., Chédin, A., Matsueda, H., MacHida, T., Armante, R., and Scott, N.A. (2009). First year of upper tropospheric integrated content of CO_2 from IASI hyperspectral infrared observations. Atmos. Chem. Phys. *9*, 4797–4810. https://doi.org/10.5194/acp-9-4797-2009.

Crisp, D., Atlas, R.M., Breon, F.M., Brown, L.R., Burrows, J.P., Ciais, P., Connor, B.J., Doney, S.C., Fung, I.Y., Jacob, D.J., et al. (2004). The orbiting carbon observatory (OCO) mission. Adv. Space Res. *34*, 700–709. https://doi.org/10.1016/j.asr.2003.08.062.

Cui, Y., Schubert, B.A., and Jahren, A.H. (2020). A 23 m.y. record of low atmospheric CO_2. Geology *48*, 888–892. https://doi.org/10.1130/G47681.1.

Ekwurzel, B., Boneham, J., Dalton, M.W., Heede, R., Mera, R.J., Allen, M.R., and Frumhoff, P.C. (2017). The rise in global atmospheric CO_2, surface temperature, and sea level from emissions traced to major carbon producers. Clim. Change *144*, 579–590. https://doi.org/10.1007/s10584-017-1978-0.

Eldering, A., Wennberg, P.O., Crisp, D., Schimel, D.S., Gunson, M.R., Chatterjee, A., Liu, J., Schwandner, F.M., Sun, Y., O'Dell, C.W., et al. (2017). The Orbiting Carbon Observatory-2 early science investigations of regional carbon dioxide fluxes. Science *358*, eaam5745. https://doi.org/10.1126/science.aam5745.

Forkel, M., Dorigo, W., Lasslop, G., Chuvieco, E., Hantson, S., Heil, A., Teubner, I., Thonicke, K., and Harrison, S.P. (2019). Recent global and regional trends in burned area and their compensating environmental controls. Environ. Res. Commun. *1*, 051005. https://doi.org/10.1088/2515-7620/ab25d2.

Foster, G.L., Royer, D.L., and Lunt, D.J. (2017). Future climate forcing potentially without precedent in the last 420 million years. Nat. Commun. *8*, 14845. https://doi.org/10.1038/ncomms14845.

Foucher, P.Y., Chédin, A., Armante, R., Boone, C., Crevoisier, C., and Bernath, P. (2011). Carbon dioxide atmospheric vertical profiles retrieved from space observation using ACE-FTS solar occultation instrument. Atmos. Chem. Phys. *11*, 2455–2470. https://doi.org/10.5194/acp-11-2455-2011.

Gunter, W.D., Wong, S., Cheel, D.B., and Sjostrom, G. (1998). Large CO_2 sinks: their role in the mitigation of greenhouse gases from an international, national (Canadian) and provincial (Alberta) perspective. Appl. Energy *61*, 209–227. https://doi.org/10.1016/S0306-2619(98)00042-7.

Gupta, A., Dhaka, S.K., Matsumi, Y., Imasu, R., Hayashida, S., and Singh, V. (2019). Seasonal and annual variation of AIRS retrieved CO_2 over India during 2003–2011. J. Earth Syst. Sci. *128*, 92. https://doi.org/10.1007/s12040-019-1108-7.

Hegerl, G.C., Crowley, T.J., Hyde, W.T., and Frame, D.J. (2006). Climate sensitivity constrained by temperature reconstructions over the past seven centuries. Nature *440*, 1029–1032. https://doi.org/10.1038/nature04679.

Houghton, R.A. (1998). The annual net flux of carbon to the atmosphere from changes in land use 1850-1990. Tellus B Chem. Phys. Meteorol. *51*, 298–313. https://doi.org/10.3402/tellusb.v51i2.16288.

IPCC (2007). In Climate change 2007-the physical science basis: Working group I contribution to the fourth assessment report of the IPCC, S. Solomon, D. Qin, M. Manning, Z. Chen, M. Marquis, K.B. Averyt, M. Tignor, and H.L. Miller, eds. (Cambridge University Press).

IPCC (2014). In Climate change 2014: Synthesis report, Contribution of working groups I, II and III to the fifth assessment report of the intergovernmental panel on climate change, Core Writing Team., R.K. Pachauri, and L.A. Meyer, eds. (IPCC Geneva).

IPCC (2021). In Climate Change 2021: The Physical Science Basis. Contribution of Working Group I to the Sixth Assessment Report of the Intergovernmental Panel on Climate Change [Masson-Delmotte, V.P. Zhai, A. Pirani, S.L. Connors, C. Péan, S. Berger, N. Caud, Y. Chen, L. Goldfarb, and M.I. Gomis, et al., eds. (Cambridge University Press). https://doi.org/10.1017/9781009157896.

Jackson, R.B., Le Quéré, C., Andrew, R.M., Canadell, J.G., Peters, G.P., Roy, J., and Wu, L. (2017). Warning signs for stabilizing global CO_2 emissions. Environ. Res. Lett. *12*, 110202–110205. https://doi.org/10.1088/1748-9326/aa9662.

Krishnapriya, M., Nayak, R.K., Allahudeen, S., Bhuvanachandra, A., Dadhwal, V.K., Jha, C.S., Sheshasai, M.V.R., Sasmal, S.K., and Prasad, K.V.S.R. (2020). Seasonal variability of tropospheric CO_2 over India based on model simulation, satellite retrieval and in-situ observation. J. Earth Syst. Sci. *129*, 211. https://doi.org/10.1007/s12040-020-01478-x.

Kulawik, S.S., Jones, D.B.A., Nassar, R., Irion, F.W., Worden, J.R., Bowman, K.W., MacHida, T., Matsueda, H., Sawa, Y., Biraud, S.C., et al. (2010). Characterization of tropospheric emission spectrometer (TES) CO_2 for carbon cycle science. Atmos. Chem. Phys. *10*, 5601–5623. https://doi.org/10.5194/acp-10-5601-2010.

Kulawik, S.S., Worden, J.R., Wofsy, S.C., Biraud, S.C., Nassar, R., Jones, D.B.A., Olsen, E.T., Jimenez, R., Park, S., Santoni, G.W., et al. (2013). Comparison of improved Aura tropospheric emission spectrometer CO_2 with HIPPO and SGP aircraft profile measurements. Atmos. Chem. Phys. *13*, 3205–3225. https://doi.org/10.5194/acp-13-3205-2013.

Kuttippurath, J., Singh, A., Dash, S.P., Mallick, N., Clerbaux, C., Van Damme, M., Clarisse, L., Coheur, P.F., Raj, S., Abbhishek, K., and Varikoden, H. (2020). Record high levels of atmospheric ammonia over India: spatial and temporal analyses. Sci. Total Environ. *740*, 139986. https://doi.org/10.1016/j.scitotenv.2020.139986.

Kuttippurath, J., Patel, V.K., Pathak, M., and Singh, A. (2022). Improvements in SO2 pollution in India: role of technology and environmental regulations. Environ. Sci. Pollut. Res. https://doi.org/10.1007/s11356-022-21319-2.

Kuze, A., Suto, H., Nakajima, M., and Hamazaki, T. (2009). Thermal and near infrared sensor for carbon observation Fourier-transform spectrometer on the Greenhouse Gases Observing Satellite for greenhouse gases monitoring. Appl. Opt. *48*, 6716–6733. https://doi.org/10.1364/AO.48.006716.

Le Quéré, C., Raupach, M.R., Canadell, J.G., Marland, G., Bopp, L., Ciais, P., Conway, T.J., Doney, S.C., Feely, R.A., Foster, P., et al. (2009). Trends in the sources and sinks of carbon dioxide. Nat. Geosci. *2*, 831–836. https://doi.org/10.1038/ngeo689.

Le Quéré, C., Jackson, R.B., Jones, M.W., Smith, A.J.P., Abernethy, S., Andrew, R.M., De-Gol, A.J., Willis, D.R., Shan, Y., Canadell, J.G., et al. (2020). Temporary reduction in daily global CO_2 emissions during the COVID-19 forced confinement. Nat. Clim. Chang. *10*, 647–653. https://doi.org/10.1038/s41558-020-0797-x.

Li, B., Shi, Y., Hao, J., Ma, C., Pang, C., and Yang, H. (2022). Research on a carbon emission calculation model and method for an underground fully mechanized mining process. Energies *15*, 2871. https://doi.org/10.3390/en15082871.

Mahesh, P., Sreenivas, G., Rao, P.V.N., and Dadhwal, V.K. (2016). Atmospheric CO_2 retrieval from ground based FTIR spectrometer over Shadnagar, India. Atmos. Meas. Tech. Discuss. *16*, 1–10. https://doi.org/10.5194/amt-2016-177.

Miller, C.E., Crisp, D., DeCola, P.L., Olsen, S.C., Randerson, J.T., Michalak, A.M., Alkhaled, A., Rayner, P., Jacob, D.J., Suntharalingam, P., et al. (2007). Precision requirements for space-based XCO_2 data. J. Geophys. Res. Atmos. *112*, 1–19. https://doi.org/10.1029/2006JD007659.

Morino, I., Uchino, O., Inoue, M., Yoshida, Y., Yokota, T., Wennberg, P.O., Toon, G.C., Wunch, D., Roehl, C.M., Notholt, J., et al. (2011). Preliminary validation of column-averaged volume mixing ratios of carbon dioxide and methane retrieved from GOSAT short-wavelength infrared spectra. Atmos. Meas. Tech. *4*, 1061–1076. https://doi.org/10.5194/amt-4-1061-2011.

Nayak, R.K., Dadhwal, V.K., Majumdar, A., Patel, N.R., and Dutt, C.B.S. (2011). Variability of Atmospheric CO_2 over India and surrounding oceans and control by surface fluxes. Int. Arch.

Photogramm. Remote Sens. Spat. Inf. Sci. *XXXVIII-8*, 96–101. https://doi.org/10.5194/isprsarchives-xxxviii-8-w20-96-2011.

Olivier, J.G.J., and Peters, J.A.H.W. (2019). Trends in Global CO_2 and Total Greenhouse Gas Emissions (PBL Netherlands Environmental Assessment Agency).

Oza, M., and Kishtawal, C.M. (2014). Spatial analysis of Indian summer monsoon rainfall. J. Geomat. *8*, 41–47.

Pasha, S.V., Behera, M.D., Mahawar, S.K., Barik, S.K., and Joshi, S.R. (2020). Assessment of shifting cultivation fallows in Northeastern India using Landsat imageries. Trop. Ecol. *611*, 65–75. https://doi.org/10.1007/S42965-020-00062-0.

Patel, V.K., and Kuttippurath, J. (2022). Significant increase in water vapour over India and Indian Ocean: implications for tropospheric warming and regional climate forcing. Sci. Total Environ. *838*, 155885. https://doi.org/10.1016/j.scitotenv.2022.155885.

Patra, P.K., Canadell, J.G., Houghton, R.A., Piao, S.L., Oh, N.H., Ciais, P., Manjunath, K.R., Chhabra, A., Wang, T., Bhattacharya, T., et al. (2013). The carbon budget of South Asia. Biogeosciences *10*, 513–527. https://doi.org/10.5194/bg-10-513-2013.

Patra, P.K., Law, R.M., Peters, W., Rödenbeck, C., Takigawa, M., Aulagnier, C., Baker, I., Bergmann, D.J., Bousquet, P., Brandt, J., et al. (2008). TransCom model simulations of hourly atmospheric CO_2: analysis of synoptic-scale variations for the period 2002–2003. Global Biogeochem. Cycles *22*, 1–16. https://doi.org/10.1029/2007GB003081.

Patra, P.K., Niwa, Y., Schuck, T.J., Brenninkmeijer, C.A.M., MacHida, T., Matsueda, H., and Sawa, Y. (2011). Carbon balance of South Asia constrained by passenger aircraft CO_2 measurements. Atmos. Chem. Phys. *11*, 4163–4175. https://doi.org/10.5194/acp-11-4163-2011.

Peter, R., Kuttippurath, J., Chakraborty, K., and Sunanda, N. (2021). Temporal evolution of mid-tropospheric CO_2 over the Indian Ocean. Atmos. Environ. *257*, 118475. https://doi.org/10.1016/j.atmosenv.2021.118475.

Preethi, B., Revadekar, J.V., and Kripalani, R.H. (2011). Anomalous behaviour of the Indian summer monsoon 2009. J. Earth Syst. Sci. *120*, 783–794. https://doi.org/10.1007/s12040-011-0112-3.

Raj, S., Paul, S.K., Chakraborty, A., and Kuttippurath, J. (2020). Anthropogenic forcing exacerbating the urban heat islands in India. J. Environ. Manage. *257*, 110006. https://doi.org/10.1016/J.JENVMAN.2019.110006.

Sanghavi, S., Nelson, R., Frankenberg, C., and Gunson, M. (2020). Aerosols in OCO-2/GOSAT retrievals of XCO_2: an information content and error analysis. Remote Sens. Environ. *251*, 112053. https://doi.org/10.1016/j.rse.2020.112053.

Schneising, O., Bergamaschi, P., Bovensmann, H., Buchwitz, M., Burrows, J.P., Deutscher, N.M., Griffith, D.W.T., Heymann, J., Macatangay, R., Messerschmidt, J., et al. (2012). Atmospheric greenhouse gases retrieved from SCIAMACHY: comparison to ground-based FTS measurements and model results. Atmos. Chem. Phys. *12*, 1527–1540. https://doi.org/10.5194/acp-12-1527-2012.

Sharma, N., Nayak, R.K., Dadhwal, V.K., Kant, Y., and Ali, M.M. (2013). Temporal variations of atmospheric CO_2 in Dehradun, India during 2009. Air Soil Water Res. *6*, 37–45. https://doi.org/10.4137/ASWR.S10590.

Sharma, N., Dadhwal, V.K., Kant, Y., Mahesh, P., Mallikarjun, K., Gadavi, H., Sharma, A., and Ali, M.M. (2014). Atmospheric CO_2 variations in two contrasting environmental sites over India. Air Soil. Water Res. *7*, 61–68. https://doi.org/10.4137/ASWR.S13987.

Shi, Y., Matsunaga, T., and Noda, H. (2017). Interpreting temporal changes of atmospheric CO_2 over fire affected regions based on GOSAT observations. IEEE Geosci. Remote Sens. Lett. *14*, 77–81. https://doi.org/10.1109/LGRS.2016.2627056.

Sikarwar, V.S., Reichert, A., Jeremias, M., and Manovic, V. (2021). COVID-19 pandemic and global carbon dioxide emissions: a first assessment. Sci. Total Environ. *794*, 148770. https://doi.org/10.1016/j.scitotenv.2021.148770.

Singh, A., Kuttippurath, J., Abbhishek, K., Mallick, N., Raj, S., Chander, G., and Dixit, S. (2021). Biogenic link to the recent increase in atmospheric methane over India. J. Environ. Manage. *289*, 112526. https://doi.org/10.1016/j.jenvman.2021.112526.

Singh, A., Abbhishek, K., Kuttippurath, J., Raj, S., Mallick, N., Chander, G., and Dixit, S. (2022). Decadal variations in CO_2 during agricultural seasons in India and role of management as sustainable approach. Environ. Technol. Innov. *27*, 102498. https://doi.org/10.1016/j.eti.2022.102498.

Sioris, C.E., Boone, C.D., Nassar, R., Sutton, K.J., Gordon, I.E., Walker, K.A., and Bernath, P.F. (2014). Retrieval of carbon dioxide vertical profiles from solar occultation observations and associated error budgets for ACE-FTS and CASS-FTS. Atmos. Meas. Tech. *7*, 2243–2262. https://doi.org/10.5194/amt-7-2243-2014.

Smith, P., Martino, D., Cai, Z., Gwary, D., Janzen, H., Kumar, P., McCarl, B., Ogle, S., O'Mara, F., Rice, C., et al. (2007). Policy and technological constraints to implementation of greenhouse gas mitigation options in agriculture. Agric. Ecosyst. Environ. *118*, 6–28. https://doi.org/10.1016/j.agee.2006.06.006.

Tiwari, Y.K., Patra, P.K., Chevallier, F., Francey, R.J., Paul, B., Allison, C.E., Revadekar, J.V., Chakraborty, S., Langenfelds, R.L., Bhattacharya, S.K., et al. (2011). Carbon dioxide observations at cape Rama, India for the period 1993–2002: implications for constraining Indian emissions. Curr. Sci. *101*, 1562–1568. http://www.jstor.org/stable/24080696.

Tiwari, Y.K., Revadekar, J.V., and Ravi Kumar, K. (2013). Variations in atmospheric Carbon Dioxide and its association with rainfall and vegetation over India. Atmos. Environ. *68*, 45–51. https://doi.org/10.1016/j.atmosenv.2012.11.040.

Thompson, R.L., Patra, P.K., Chevallier, F., Maksyutov, S., Law, R.M., Ziehn, T., Van Der Laan-Luijkx, I.T., Peters, W., Ganshin, A., Zhuravlev, R., et al. (2016). Top-down assessment of the Asian carbon budget since the mid-1990s. Nat. Commun. *7*, 10724. https://doi.org/10.1038/ncomms10724.

Valsala, V., Tiwari, Y.K., Pillai, P., Roxy, M., Maksyutov, S., and Murtugudde, R. (2013). Intraseasonal variability of terrestrial biospheric CO_2 fluxes over India during summer monsoons. J. Geophys. Res. Biogeosci. *118*, 752–769. https://doi.org/10.1002/jgrg.20037.

van der Werf, G.R., Morton, D.C., DeFries, R.S., Olivier, J.G.J., Kasibhatla, P.S., Jackson, R.B., Collatz, G.J., and Randerson, J.T. (2009). CO_2 emissions from forest loss. Nat. Geosci. *2*, 737–738. https://doi.org/10.1038/ngeo671.

Venkataraman, C., Habib, G., Kadamba, D., Shrivastava, M., Leon, J.F., Crouzille, B., Boucher, O., and Streets, D.G. (2006). Emissions from open biomass burning in India: integrating the inventory approach with high-resolution Moderate Resolution Imaging Spectroradiometer (MODIS) active-fire and land cover data. Global Biogeochem. Cycles *20*, 1–12. https://doi.org/10.1029/2005GB002547.

Wang, M. (1999). Atmospheric Chemistry, 2nd Edition (China Meteorological Press), pp. 144–147.

Wunch, D., Wennberg, P.O., Osterman, G., Fisher, B., Naylor, B., Roehl, C.M., O'Dell, C., Mandrake, L., Viatte, C., Kiel, M., et al. (2017). Comparisons of the orbiting carbon observatory-2 (OCO-2) XCO_2 measurements with TCCON. Atmos. Meas. Tech. *10*, 2209–2238. https://doi.org/10.5194/amt-2016-227.

Yang, Y., and Zhao, Y. (2019). Quantification and evaluation of atmospheric pollutant emissions from open biomass burning with multiple methods: a case study for Yangtze River Delta region, China. Atmos. Chem. Phys. *19*, 327–348. https://doi.org/10.5194/acp-19-327-2019.

Yang, H., Feng, G., Xiang, R., Xu, Y., Qin, Y., and Li, S. (2020). Spatio-temporal validation of AIRS CO_2 observations using GAW, HIPPO and TCCON. Remote Sens. (Basel). *12*, 3583. https://doi.org/10.3390/rs12213583.

Yoshida, Y., Kikuchi, N., and Yokota, T. (2012). On-orbit radiometric calibration of SWIR bands of TANSO-FTS onboard GOSAT. Atmos. Meas. Tech. *5*, 2515–2523. https://doi.org/10.5194/amt-5-2515–2012.

STAR★METHODS

KEY RESOURCES TABLE

REAGENT or RESOURCE	SOURCE	IDENTIFIER
Deposited data		
Atmospheric InfraRed Sounder (AIRS) CO_2 Data	JPL	https://airs.jpl.nasa.gov/
GOSAT CO_2 Data	NIES	https://data2.gosat.nies.go.jp/GosatDataArchiveService/
SCIAMACHY CO_2 Data		https://www.iup.uni-bremen.de/sciamachy/NIR_NADIR_WFM_DOAS/products/
OCO-2 CO_2 Data	JPL	https://ocov2.jpl.nasa.gov/
MERRA-2 Data	GSFC	https://gmao.gsfc.nasa.gov/reanalysis/MERRA-2/
MODIS NDVI data	GSFC	https://neo.sci.gsfc.nasa.gov/view.php?datasetId=MOD_NDVI_M
Population data	SEDAC	https://sedac.ciesin.columbia.edu/data/collection/gpw-v4
Burned area data	CCI	https://geogra.uah.es/fire_cci/firecci51.php

RESOURCE AVAILABILITY

Lead contact

Further information and requests for resources should be directed to and will be fulfilled by the Lead Contact, Jayanarayanan Kuttippurath (jayan@coral.iitkgp.ac.in).

Materials availability

This study did not generate any new dataset.

Data and code availability

- Data: This paper uses existing publicly available data. These datasets are listed in the key resources table.
- Code: This paper does not report any original code. However, the codes used for analysis are written in Stata and R, and are available from the lead contact upon request.
- Additional information: Any additional information required to reanalyse the data reported in this paper is available from the lead contact upon request.

METHOD DETAILS

Datasets

We have used atmospheric CO_2 retrieved from different satellite measurements, AIRS, GOSAT, SCIAMACHY, and OCO-2, as available publicly. AIRS is an Infrared spectrometer that operates at 3.7–15.4 μm (Aumann et al., 2003). This near-polar orbiting sun-synchronous satellite measures daily CO_2 with global coverage over the land and ocean. The mid-tropospheric CO_2 is retrieved with the maximum sensitivity at 500–300 hPa (Chahine et al., 2005). We have taken the measurements from September 2002 to February 2017. The horizontal resolution is 2.5 × 2° and is accurate to 1–2 ppm compared to other independent measurements (Chahine et al., 2008; Yang et al., 2020).

The sun-synchronous GOSAT was launched in 2009 to observe the atmospheric abundance of CO_2 and CH_4, which orbits at an altitude of 666 km with a revolution period of 100 min. It accommodates two instruments, TANSO-FTS and the TANSO Cloud and Aerosol Imager radiometer. The spectrometer detects the

reflected SWIR and TIR from the surface and atmosphere (Kuze et al., 2009; Morino et al., 2011). We have used the L3 global CO_2 data (SWIR) version 2.81 provided by NIES for the period 2009–2020. These data have a spatial resolution of 2.5 × 2.5° and an accuracy of about 2 ppm or 0.5% (Morino et al., 2011).

SCIAMACHY is an eight-channel spectral grating instrument that detects the reflected radiation at 240–2400 nm and has a spatial resolution of 30 × 60 km^2 (Bovensmann et al., 1999). The Weighting Function Modified Differential Absorption Spectroscopy (WFM-DOAS) algorithm was used to retrieve the CO_2 concentrations and are most sensitive near the surface. We have used the L2 column-averaged CO_2 data for the period 2002–2012. The accuracy of monthly averaged SCIAMACHY data within 500 km is about 1.1–1.2 ppm (Schneising et al., 2012).

The OCO-2 satellite is the first dedicated payload to study CO_2 from space (Eldering et al., 2017). The pole-to-pole orbiting satellite carries the OCO-2 instrument to measure the reflected sunlight in the NIR and SWIR spectra. We have considered the Level 2 data for the period 2014–2020. These data have a spatial resolution of 2.5 × 2.5° and an accuracy of 0.5–1.0 ppm (Wunch et al., 2017). Further details of the datasets are given in Table 1.

We have used the Moderate Resolution Imaging Spectroradiometer NDVI (MOD13C1), a monthly global NDVI product with 0.05° spatial resolution, for the period 2002–2020. The seasonal averages are calculated to assess the role of NDVI in regulating atmospheric CO_2 with time. The coal consumption data of India are taken from the Office of Coal Controller, Ministry of Coal, India, http://www.coalcontroller.gov.in/. The crude oil consumption data are obtained from the Ministry of Petroleum and Natural Gas, India, https://mopng.gov.in/en. The total energy consumption data are retrieved from the repository of the U.S. Energy Information Administration (EIA). The cement production data are taken from the report made by the Ministry of Commerce, India. The precipitation data from IMD (India Meteorological Department) for the period 2002–2020 are considered to examine the impact of meteorology on atmospheric distribution of CO_2. The temperature and wind data are taken from the Modern-Era Retrospective analysis for Research and Applications (MERRA-2), which has a spatial solution of about 0.625 × 0.5°. We have used the fire counts and burned area estimates from MODIS to analyze the biomass burning and its connection to atmospheric CO_2 (Forkel et al., 2019). We have also considered the population data to analyze the human impact on atmospheric emissions. Population data are taken from the report of India Census (2011) (Censusindia.gov.in).

Methods

The bias in different satellite measurements is calculated by selecting the common periods for the respective datasets and then the data are interpolated to the coarser grid between the datasets. The following overlapping years are used for the computation of biases. For GOSAT and OCO-2: September 2014 to January 2020, GOSAT and SCIAMACHY: June 2009 to April 2012, AIRS and GOSAT: June 2009 to December 2016, AIRS and OCO-2: September 2014 to December 2016, and AIRS and SCIAMACHY: October 2002 to April 2012. Note that there are only a few observations from GOSAT and OCO-2 in JJAS, which resulted in lower values as shown in the south, central and northeast India. There are six homogeneous regions in accordance with the concentrations of atmospheric CO_2 in India and Indian Ocean regions. These are: South India (SI), Central India (CI), Indo-Gangetic Plain (IGP), and Third Pole (TP). In addition, we have also considered the Arabian Sea (AS) and Bay of Bengal (BoB), although these oceanic regions are not included in further scientific discussion (Figure S5). The regional averages are discussed for monthly, seasonal, inter-annual variability, and the temporal trends in atmospheric CO_2.

QUANTIFICATION AND STATISTICAL ANALYSIS

To find the bias (i.e. difference between two measurements) in satellite CO_2 observations, a common time period of both satellite measurements is selected and the spatial resolution is set to match the lowest resolution observations. For example, to find the bias between AIRS and GOSAT measurements, the common observation period from 2009-06-01 to 2016-12-01 is considered, and the relatively high resolution AIRS (2° × 2.5°) data are regridded to the resolution of GOSAT (2.5° × 2.5°) by using a Python code. The homogeneous regions are selected based on the distribution of atmospheric CO_2 in the study area (Figure S5). The SD of each homogeneous region is calculated from the mean of the CO_2 concentration over those regions. The average CO_2 concentration represents the mean of CO_2 measurements from SCIAMACHY, AIRS, GOSAT, and OCO-2. The long-term trend in the CO_2 data are computed using the linear regression, and the significance of estimated trend is found with respect to the 95% confidence interval by applying the t–test statistics.